RSC Advances

PAPER

View Article Online
View Journal | View Issue

Cite this: *RSC Adv.*, 2019, **9**, 26637

Reduced graphene oxide/CoS_2 porous nanoparticle hybrid electrode material for supercapacitor application

Lemu Girma Beka, Xin Li, Xiaoli Wang, Chuanyu Han and Weihua Liu *

Graphene/transition metal hybrid electrode materials are considered promising electrode materials for supercapacitor applications. However, the stacking of graphene sheets and agglomeration of transition metal parts are still challenging issues to overcome in order to achieve the expected theoretical performances. Herein, a reduced graphene oxide/cobalt disulphide porous nanoparticle hybrid electrode material is fabricated using sulphur as the template precursor. The unique porosity derived from the sulphur template gives favourable open structures for easy diffusion of electrolyte ions and better accessible active sites, and free space for volume changes and results in improved electrochemical performance. In this hybrid material the graphene layers serve as a conductive matrix and physical support for pours cobalt sulphide nanoparticles. On the other hand, the porous cobalt sulphide redox-active material uniformly decorated on rGO can enhance the pseudocapacitive performance of the as synthesized hybrid material. Using the combined advantage of graphene and transition metal sulphide the as synthesized composite electrode material has excellent specific capacitance, excellent rate capability and cycling stability. Thus, our design approach can be considered as a potential candidate to design advanced energy storage devices.

Received 16th July 2019
Accepted 2nd August 2019

DOI: 10.1039/c9ra05434k

rsc.li/rsc-advances

1. Introduction

Supercapacitors (electrochemical capacitors or ultracapacitors) are energy storage devices designed to take advantage of near-surface charge storage mechanisms[1–3] to achieve excellent power density,[4] long cycling stability and improved environmental safety.[5,6] However, according to the current state-of-art the low energy density properties limit the practical application of supercapacitors in different application areas.[7] Depending on their energy storing mechanism, supercapacitors can be one of two types.[2,8] The first is an electrical double-layer capacitor (EDLC), where energy storage is dominated by electrostatic charge diffusion and accumulation at the electrode/electrolyte interface and the second is pseudocapacitors where energy storage is achieved by reversible faradaic reactions that occur at the electrode surface.[9]

Great research efforts have been in progress by different research groups to develop novel electrode materials and electrode structures using different electrode materials (carbon materials, transition metal compounds, polymers, and composite or hybrid materials).[10–17] Carbon based materials exhibit excellent electrochemical aspects like conductivity and cycling stability but suffer from low specific capacitance.[18,19] Transition metal based compounds deliver high specific capacitance which is usually 2–3 times higher than that of carbon materials.[20] However, they suffer from poor rate capability and short cycling stability. Among transition metal based electrode materials, cobalt sulphides are one of promising electrode material for supercapacitor application, due to their low cost and better electrical conductivity.[21–26] However, like other transition metal compounds transition metal sulphides also suffer from low cycling stability and low rate capability.

Hybridizing transition metal based pseudocapacitive materials with carbon materials is becoming one of the promising research direction.[27] The carbon material with excellent electron transport, large surface area, regular frameworks and strong thermal/chemical stability is expected to support different structure of pseudocapacitive materials and increase rate capability and cycling stability of the hybrid material.[28–31] On the other hand, transition metal compounds are interesting to enhance the energy density of the hybrid material by incorporating redox reaction charge storage mechanism.[32,33] Different researchers have demonstrated the enhancement in electrochemical performances of transition metal sulphides after hybridizing with graphene.[34–39] Even though numerous work on graphene/transition metal sulphide hybrid materials are reported in the literature, the stacking of graphene sheets and agglomeration of transition metal sulphides and volume changes during charge discharge are still challenging. In this regard, design of hierarchical porous nanostructure has attracted great attentions in supercapacitor electrode materials research.[40] Specially, design of porous electrode materials which can result in fast ion diffusion and electron transport and incorporation of free spaces for volume changes during charge discharge are highly needed.[41,42]

School of Microelectronics, School of Electronic and Information Engineering, Xi'an Jiaotong University, Xi'an, 710049, P. R. China. E-mail: lwhua@mail.xjtu.edu.cn

Herein, we report reduced graphene oxide/porous cobalt disulphide nanoparticle (rGO/CS) hybrid electrode material for supercapacitor application. The hybrid material is prepared by a simple hydrothermal reduction process followed by thermal annealing process. In this work, we used sulphur as a template and precursor material. The sulphur template was used to incorporate open spaces in rGO/CS hybrid electrode material. Thus, the final rGO/CS hybrid electrode material incorporates excellent conductive rGO material well-uniformly decorated with highly porous CS redox active material and resulted in excellent electrochemical performance. Using these synergistic advantages, the as prepared electrode material resulted in excellent specific capacitance of 1572 F g^{-1} at current density of 3 A g^{-1}, excellent rate capability of 105% as current increase from 1 to 20 A g^{-1} and excellent cycling stability of 92% after 2000 cycles of charge discharge and 88% after 4000 of charge discharge.

2. Experimental

2.1 Preparation of porous rGO/cobalt disulphide nanoparticle

All the reagents used in the experiment were of analytical grade and used without further processing. Pours rGO/CS was prepared by hydrothermal process followed by annealing process; the detail of preparation process is presented as follows. Step I, 0.05 g of GO was added to 25 mL of DI water and sonicated for 3 h. Step II, a solution containing 0.75 m mole of thiourea ($CS(NH_2)_2$) was added into the pre-prepared rGO solution and stirred for 1 h. Next, a homogenous solution containing $CoCl_2 \cdot 6H_2O$ and $CS(NH_2)_2$ was prepared using 10 mL of DI water and added to the pre-prepared solution of step I and stirred for additional 30 minutes. Then, the as prepared homogenous solution was transferred to a 60 mL Teflon-lined stainless steel autoclave and heated at a temperature of 180 °C for 6 h and monolith cylinder like rGO/sulphur/CS composite was obtained. After washing in DI water it was dried at a temperature of 60 °C for 24 h. Finally, the dried monolith structure was annealed using a pipe furnace at a temperature of 500 °C for 5 h and as a final product porous rGO/CS was obtained.

2.2 Structural characterization methods

To study the structure and composition of as synthesized electrode material different techniques are used, namely, Field Emission Scanning Electron Microscopy (FE-SEM, Gemini SEM 500, Zeiss, Germany), X-ray diffraction (XRD) spectra (Bruker D8 ADVANCE), and X-ray Photoelectron Spectroscopy (XPS, Thermo Fisher ESCALAB Xi+). FE-SEM and FE-TEM were used to study the topography/morphology of the as synthesized electrode materials. The XPS analysis was used to understand the surface chemical states and bonding issues in the hybrid materials. XRD test was used to study the crystal structure of the as synthesized electrode materials.

2.3 Electrochemical characterization methods

Electrochemical test was conducted using multi channel electrochemical workstation (CS 2350 Corrtest, Wuhan, China). In three electrode configuration test the active material was used as working electrode while Hg/HgO and platinum sheets were used as reference and counter electrodes, respectively. The electrochemical tests conducted using electrochemical work station are, Cyclic Voltammetry (CV) test, Galvanic charge/discharge (GCD) test and electrochemical impedance spectroscopy (EIS) tests.

In electrochemical analysis calculating the value of specific capacitance is key part. In this experiment we calculated the specific capacitance from the GCD plots. The average mass specific capacitance values in three electrode configuration can be calculated from GCD curves, using eqn (1):[43,44]

$$C_s = \frac{I \times \Delta t}{m \times \Delta u} \quad (1)$$

where, C_S (F g^{-1}) is mass specific capacitance, I (A) is discharge current, Δt (s) is discharging time, m (g) is mass of active material, and Δu (V) is operating potential window.

3. Results and discussion

3.1 Structural characterization methods

To understand the as synthesized hybrid structure it is better to first understand the growth mechanism of rGO/CS hybrid

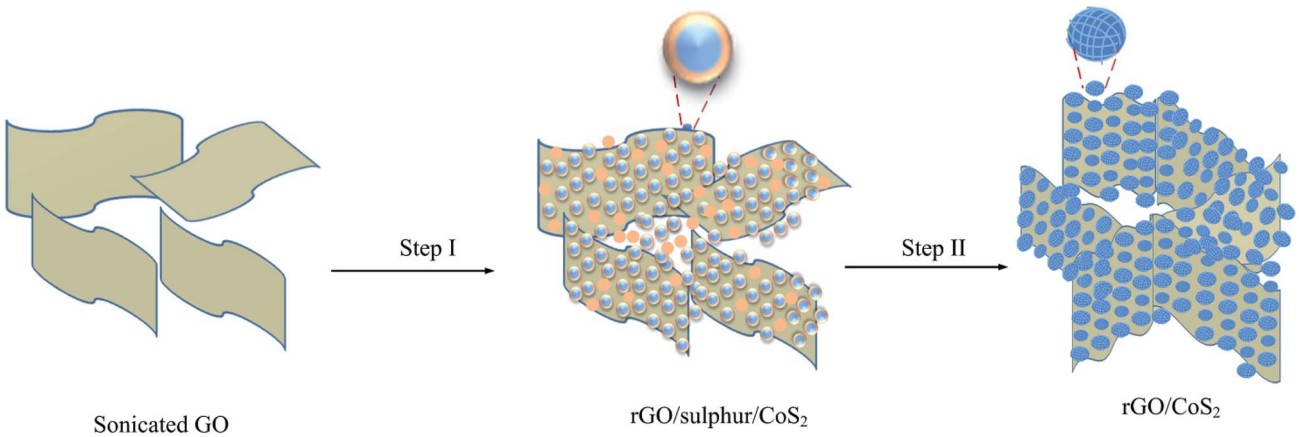

Fig. 1 Schematic illustration for preparation process of rGO/CS hybrid electrode material.

structure. Thus, the detail growth mechanism of the as synthesized hybrid material is proposed as follows (Fig. 1). Fig. 1 (Step I) spherical CoS_2 and sulphur are wrapped on the rGO surface. At this stage the nucleation of nanoparticles starts by using the functional groups on GO as a nucleation centre. Once the nucleation started at GO surface the isomerism structure of thiourea can offer an S–H bond, and the neighboring ones of isomerism can be further oxidized into S–S as shown in eqn (3). The existence of polymeric sulphur (S_n^{-2}) can reacted with Co_2^{+} forming the CoS_2 monomers (eqn (4)) and later these monomers are grown in to spherical CoS_2.[45]

The excess thiourea in this hybrid structure (which does not react with Co^{2+} cations to form CoS_2) remains warped into rGO and CoS_2 materials after the hydrothermal process. The excess thiourea used is a key material which acts as a template for formation of open and pours rGO/CS structure (Fig. 1 (step II) shows porous CS warped on rGO). During the annealing process the excessive thiourea in the composite structure is decomposed into H_2S, NH_3 and CO_2 and the bubbling out of these gaseous materials creates porous structure during this preparation process.[46] The detail facile chemical reaction of porous CS is shown in eqn (2)–(4).[47]

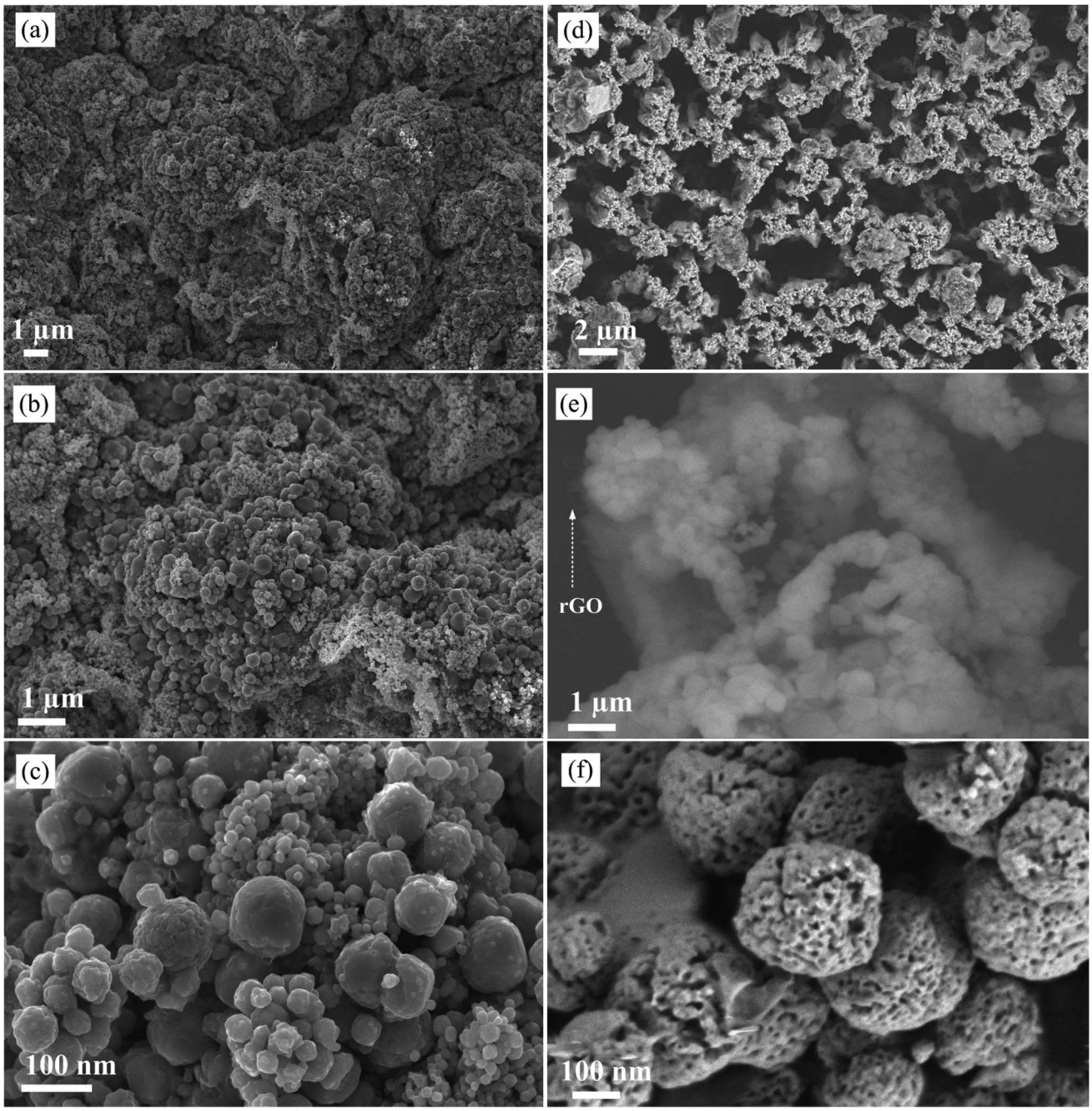

Fig. 2 (a) to (c) SEM image of rGO/CS before sulphur removal process at different magnifications and (d) to (f) SEM images of rGO/CS after sulphur removal process at different magnifications.

During the hydrothermal process the following chemical reactions will take place:

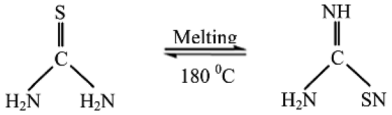

(2)

After oxidation and coordination process isomerism structure of thiourea shown in eqn (2) can offer an S–H bond, and the neighbouring ones of isomerism can be further oxidized into S–S as shown in eqn (3):

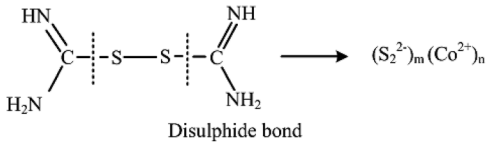

(3)

Next these disulfide bonds will react with Co^{2+} and final CoS_2 will be formed, once the monomer of CoS_2 is formed it will grow to large nanoparticles $(CoS_2)_n$.

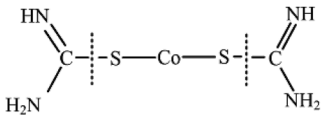

(4)

To understand the application of sulphur as a template material in rGO/CS hybrid material we conducted a comparative study before and after sulphur removal process. For simplicity sample before sulphur removal process is labelled as rGO/CS-BSR and sample after sulphur removal process is labelled as rGO/CS-ASR. Fig. 2 shows typical FE-SEM image of rGO/CS-BSR and rGO/CS-ASR at different magnifications. Fig. 2a–c shows FE-SEM image of rGO/CS-BSR. At this stage moonlight solid rGO/CS hybrid structure is obtained. It shows highly agglomerated rGO/CS hybrid materials. On the other hand, Fig. 2d–f shows FE-SEM images of rGO/CS-ASR. The solid moonlight structure shown in Fig. 2a is completely converted to open 3D structure as shown in Fig. 2d. Additionally, the nanoparticles anchored in the walls of the rGO are completely converted into porous structure (Fig. 2f) after annealing process compared to the solid nanoparticles in rGO/CS-BSR (Fig. 2c). The open structure obtained in rGO/CS after sulphur removal process

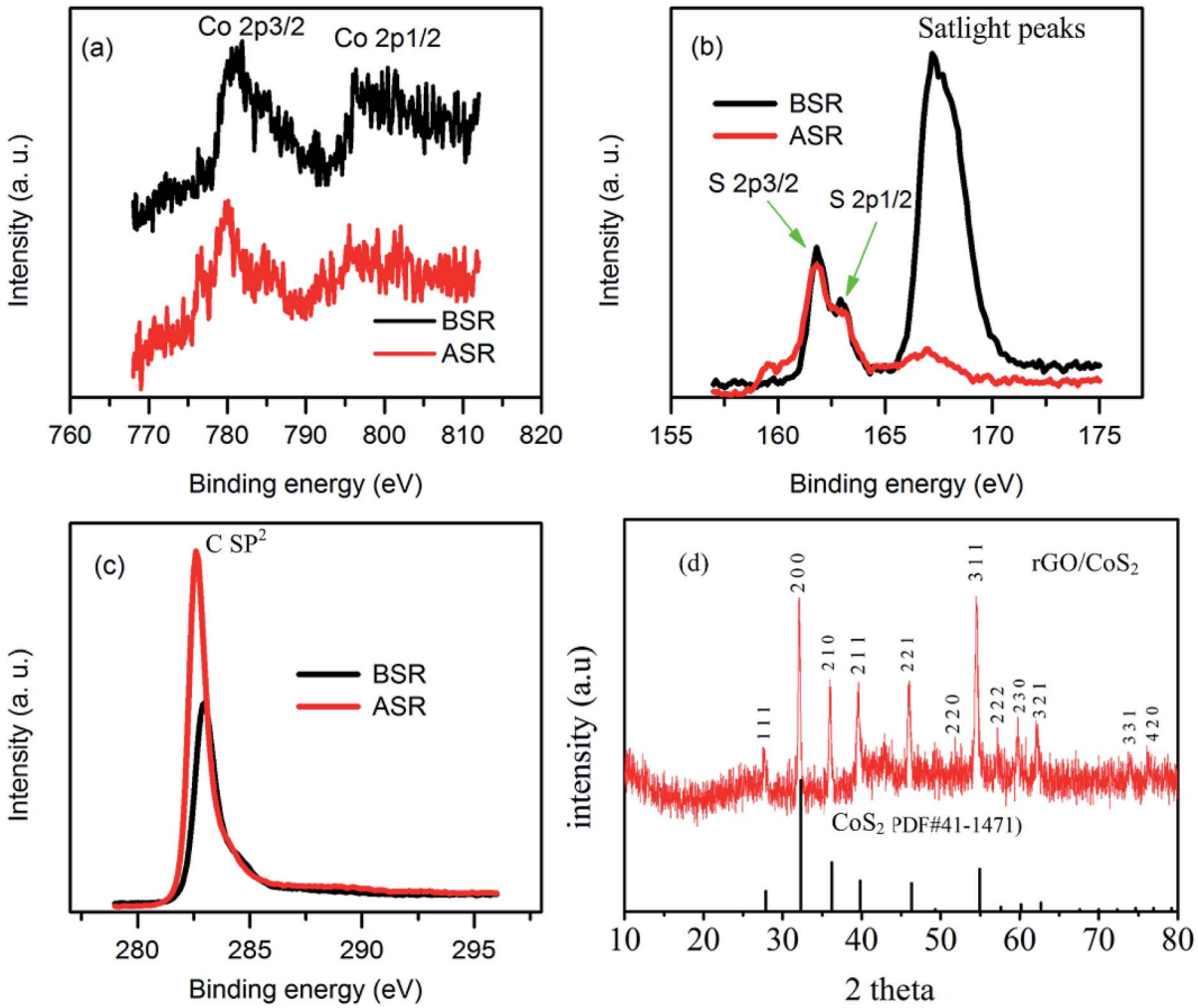

Fig. 3 XPS and XRD analysis (a) Co 2p, (b) S 2p, (c) C sp^2 and (d) XRD analysis.

clearly can facilitate better deep penetration of electrolyte ions into the hybrid structure and can enhance electrochemical performance of rGO/CS hybrid materials.

To understand the chemical states of each element in the composite before and after template removal process we conducted XPS analysis. Fig. 3 illustrates the relative XPS spectra of different elements in the composition before and after sulphur removal process. All the XPS spectra's have shown little shift after high temperature treatment illustrating the changing of chemical environments after high temperature annealing due to sulphur removal process.[48,49] Fig. 3a illustrates Co 2p spectra; the binding energies around 781 and 796 eV show Co $2p_{3/2}$ and Co $2p_{1/2}$, respectively, which are close to the reported values in the literature.[35,50] Fig. 3b illustrates S 2p spectra; it shows binding energies which can be assigned to S $2p_{3/2}$, S $2p_{1/2}$ and satellite peaks. Clearly there is large amount of sulphurs which didn't make bonding with cobalt before hydrothermal process compared to the amount of sulphur which remains after annealing process. This illustrates as excess free sulphurs are melted out and only those which make bonding with metal part and carbon remains in the hybrid material. Fig. 3c illustrates C sp^2 spectrum. Obviously, it shows one district peak around 284 eV confirming the existence of sp^2 hybridized carbon atoms illustrating existence of graphene nanosheets in the composite.[50,51] To study the crystal structure of as synthesized hybrid material we conducted XRD analysis (Fig. 3d). There are clear strong peaks around 27.8, 32.3, 36, 39.8, 46.3, 49.3 54.9 57.6, 60.1, and 62.7° which can be indexed to crystal plane of (111), (200), (210), (211), (220), (221), (311), (222), (230) and (231). Clearly, the diffraction peaks can be well related to the standard crystal phase of CoS_2 (PDF#41-1471). The non existence of other peaks illustrates as pure phase material is prepared. As it can be seen from XRD analysis the rGO part is not clearly seen this may be related to the high amount of the CoS_2 parts dominating the hybrid material, indicating as the graphene sheets are wrapped with CoS_2 and remain in exfoliated state.[52] To study the distribution of elements in the composite we conducted elemental mapping analysis and the result is shown in Fig. 4. Clearly, the final product showed uniform distribution of carbon, cobalt and sulphur elements in the composite.

3.2 Electrochemical characterization

Fig. 5 shows the electrochemical test result of as synthesized 3D rGO/CS hybrid electrode material. Fig. 5a shows the CV plots at different scan rates from 3 to 15 mV s^{-1} within potential window of 0 to 0.6 V. Clearly, the as synthesized hybrid material showed a pair of redox peaks illustrating pseudocapacitive

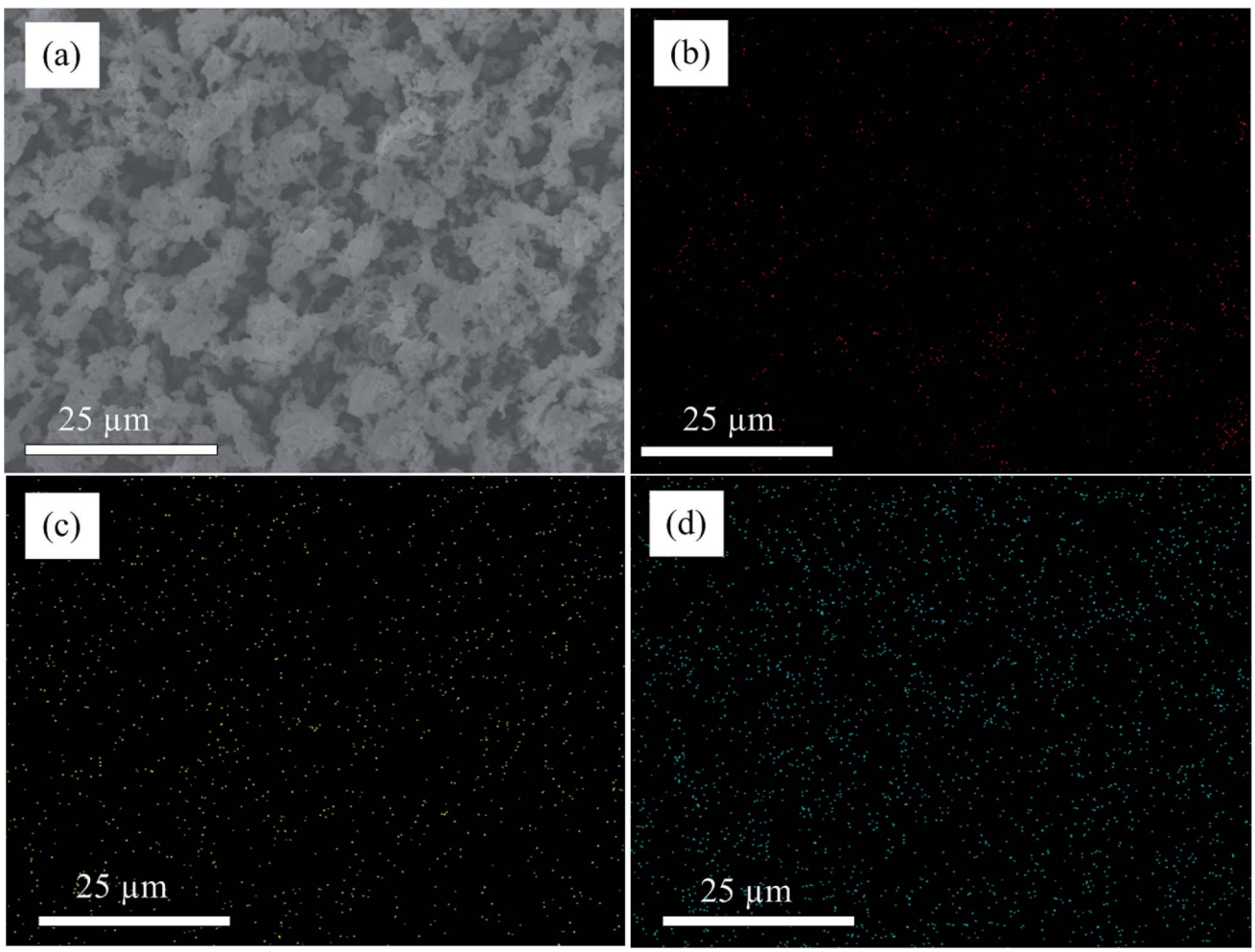

Fig. 4 Elemental mapping of rGO/CoS_2 (a) SEM images where elemental mapping taken, (b) carbon, (c) cobalt and (d) sulphur.

property. The relative GCD plots of as synthesized samples are also shown in Fig. 5b. All the GCD plots have shown plateaus region on their respective graphs illustrating pseudocapacitive property which is in agreement with the CV graphs. Both the CV and GCD plots showed symmetric property during charging and discharging process and illustrate excellent reversibility of as synthesized active material. The specific capacitance of as synthesized hybrid sample is calculated from GCD graphs using eqn (1). The calculated specific capacitance at different current densities are 1289.5, 1340, 1572, 1554, 1470, 1490 F g^{-1} at current densities of 1, 1.5, 3, 5 and 10 A g^{-1}, respectively. The as synthesized material showed highest specific capacitance of 1572 at current density of 3 A g^{-1}. The increase of specific capacitance from 1289.5 to 1572 F g^{-1} when current density increased from 1 to 3 A g^{-1} maybe due to the activation of active materials as current density is increased. Fig. 5c shows the plot of specific capacitance as a function of current density.

In supercapacitor research, rate capability is very important issue. As current density increased from 1 to 20 A g^{-1} 105% of capacitance is retained. This excellent performance can be directly related to the 3D open structure of as synthesized hybrid structure which can make deep penetration of electrolyte and facilitates easy diffusion of ions at high current density. In supercapacitor design, investigating cycling stability is also another important issue. In this regard we conducted a cycling test by applying a constant current density of 5 A g^{-1}. Clearly, after 2000 cycles of charge discharge the capacitance values remains at 92% and 88% after 4000 of charge discharge. This excellent cycling stability can be related to structure of CS decorated on rGO and the structure of rGO to support the physical stress during continues charge discharge process in the following aspects. (1) Porous CS are uniformly distributed on the rGO surface and resulted in uniform distribution of current density along the composites; (2) the porosity structure

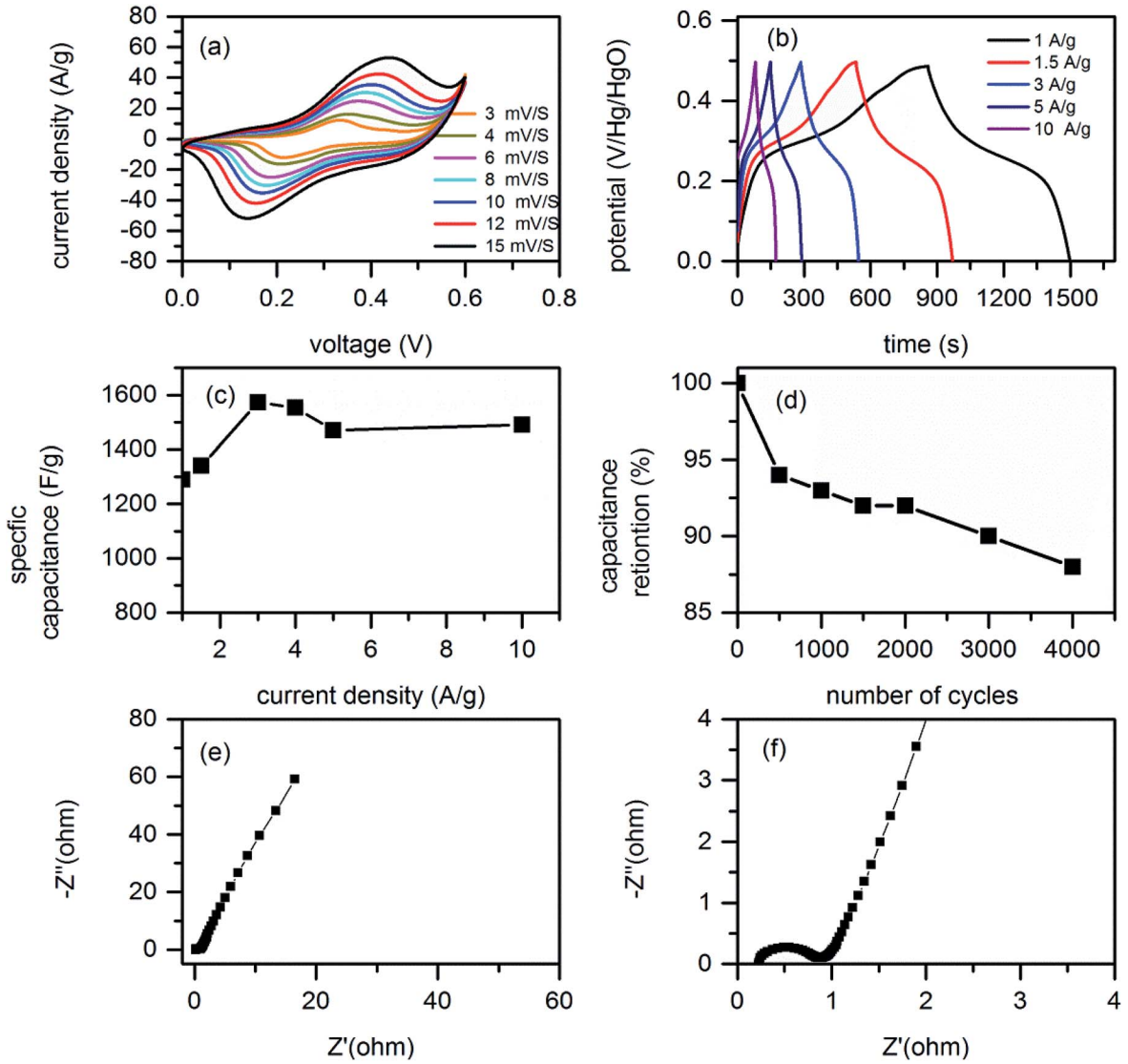

Fig. 5 Electrochemical test results of rGO/CS (a) CV plots at scan rates ranging from 3 to 15 mV s^{-1}, (b) GCD plots at different current densities, (c) specific capacitance (F g^{-1}) as a function of current density, (d) cycling stability, (e) EIS plots at low frequency region and (f) EIS plots at high frequency region.

in CS enables free space to accommodate volume changes during charging discharging process. (3) The rGO in the hybrid material is excellent flexible substrate to support volume changes and stress during charge discharge process and resulted in good cycling stability.

To understand electrochemical reaction kinetics related to ion and electron transport issues we conducted EIS study. The EIS result is plotted in Fig. 5e and f. In EIS plots, the inclined line illustrates excellent ion transports while the least inclination angle shows less ion transportation characteristics. As we can see form Fig. 5e, our rGO/CS showed good slope implying better ion transportation rate. Moreover, the high frequency impedance characteristic is shown in Fig. 5f. In EIS plot samples having smaller semi-circle diameters illustrates high charge transfer characteristics at electrode electrolyte interface. In our rGO/CS the open structure facilitates easy transportation of electrolyte ions while the rGO part facilitates electron transport during charge discharge process and ensures an improved electrode kinetics and mass transport.

In general, compared to recent reports (Table 1) our rGO/CS has shown excellent electrochemical performances. To clearly elaborate the performance of the as synthesized material we did a comparison test with cobalt sulfides reported with and without rGO. Clearly as we can see from Table 1 samples with rGO has showed better performance compared to pristine samples; this can be related to excellent properties of rGO as physical support to facilitate electrical conductivity and effective utilizations of active materials. Additionally the excellent thermal/chemical stability of rGO enhanced the cycling capability of these hybrid materials. The key question need to be answered here is why performance difference is observed between samples hybridized with rGO and in particular why our material outperforms the other reports hybridized with rGO? The answer is related to the structure/morphology of as synthesized hybrid materials. Structure/morphology of transition metal sulphide decorated on graphene and the structure/morphology of graphene on which the transition metal sulphide decorated unquestionably play key role on electrochemical performance of rGO/transition metal sulphide electrode materials. Thus the performance difference observed in this report is directly related to structure morphology of as synthesized material. In our design we used sulphur as a template material and we introduced porosity to the as synthesized hybrid materials. This porous structure can facilitate deep penetration of electrolyte ions to access better active sites and leads to maximized utilization of active materials and leads to improved capacitance compared rGO/cobalt sulphides reported in the literatures. We also tried to compare the rate capability of our material with reported literatures as shown in Table 1. Clearly, our hybrid material showed 105% capacitance retention as current density is increased from 1 to 20 A g^{-1} which is by far better than the reported materials listed in Table 1. The higher capacitance at both low current density and high current densities can illustrate as the electrolyte ions have sufficient time to diffuse into the active materials at both high and low current densities. As we have seen in the SEM images (Fig. 2e and f) both the rGO/CS frame works and the nanoparticles are porous structure which can facilitates easy diffusion of ions at both low and high current density. Thus, the sulphur template enables to obtain porous structure and avoids the agglomeration of samples and better rate capability is obtained compared with other reported literatures. The other relative comparison we did is cycling stability. As we can see from Table 1 the cycling stability reported in most literatures is for less than 2000 cycles of charge discharge. Relatively our sample has shown good cycling stability of 92% after 2000 cycles of charge discharge and 88% after 4000 cycles of charge discharge which is better than most of the reported materials. This good cycling stability can be related to the following points. (1) The cobalt sulphide nanoparticles are uniformly distributed on the rGO surface and resulted in uniform distribution of current density along the composites; (2) the rGO in the hybrid material is excellent flexible substrate to support volume changes and stress during charge discharge process and resulted in good cycling stability. (3) The porosity structure in cobalt sulphide nanoparticles accommodate volume changes during charging discharging process and good cycling stability is obtained.

Table 1 Comparison of electrochemical performance of our rGO/CS with reported literatures

Electrode material	Specific capacitance (F g^{-1}, A g^{-1})	Retention rate (%, A g^{-1})	Capacitance retained (%), cycles, current (A g^{-1})	Reference
$NiCo_2S_4$ porous nanotube	933, 1	58.95, 1 to 5	63, 1000, 1	25
Nickel cobalt sulfide	1036, 1	65.08, 1 to 20	87, 2000, 5	26
3D cauliflower-like $NiCo_2S_4$	1471, 1 A g^{-1}	86.5, 1 to 20	94.9, 1000, 10	53
$NiCo_2S_4$ nanoparticles	1440, 3	75.1, 2 to 50	107.9, 1000, 3	54
$CoNi_2S_4/Co_9S_8$	1183.3, 2	74.9, 2 to 20	97.3, 1000, 12	55
Cockscomb $NiCo_2S_4$	968, 1	74, 1 to 20	89, 4000	56
Acetylene black-$NiCo_2S_4$	768, 2	80, 2 to 20	—	57
CoS_2 nanocrystals	654, 0.5	76, 0.5 to 5	72, 600	45
$CoNi_2S_4$–G–$MoSe_2$	1141, 1	50.8, 20	108, 2000, 20	58
$CuCo_2S_4$/graphene C	665, 7.5	87.06, 5 to 10	83, 1000, 4	59
$NiCo_2S_4$/rGO	1498, 1	72.3, 40	89.1, 10, 000	60
$NiCo_2S_4$/rGO	1451, 3	52.3, 20	76.36, 2000, 5	61
$CoNi_2S_4$-rGO	1390, 1	62, 1 to 20	57, 5	62
rGO/CoS_2	1572, 3	105, 1 to 20	92, 2000, 5 88, 4000, 5	This work

4. Conclusions

In summary, we reported porous rGO/CS hybrid electrode material using sulphur as template precursor. The porous nano sized CS redox-active material density decorated on rGO ensures improved electrode kinetics. Additionally, the unique porosity derived from sulphur template resulted in better accessible active sites and fast and favourable diffusion of ions along electrode materials. On the other hand, graphene layers in the composite provide a highly conductive matrix for CS and also suppress the volume change and agglomeration of CS. Thus, using these synergistic advantages the as synthesized hybrid electrode material has shown excellent electrochemical performance of 1572 F g^{-1} at current density of 3 A g^{-1}, with excellent rate capability of 105% after current increased from 1 to 20 A g^{-1} and excellent cycling stability of 92% after 2000 cycles of charge discharge and 88% after 4000 of charge discharge. This kind of hierarchical porous composite electrode material may show great potential for advanced energy storage devices in future.

Conflicts of interest

The authors state as "There are no conflicts to declare".

Acknowledgements

The financial support of this work is by China Post-doctoral Science Foundation (Grant No. 2018M633511), the National Natural Science Foundation (Grant No. 61671368, 61172041, 91123018 and 61404103) and the Fundamental Research Funds for the Central Universities.

Notes and references

1 A. Burke, *J. Power Sources*, 2000, **91**, 2037–2050.
2 B. E. Conway, *Electrochemical supercapacitors: scientific fundamentals and technological applications*, Kluwer Academic/Plenum Publisher, New York, 1999.
3 M. Winter and R. J. Brodd, *Chem. Rev.*, 2004, **104**, 4245–4269.
4 R. A. Huggins, *Solid State Ionics*, 2000, **134**, 179–195.
5 P. Simon, Y. Gogotsi and B. Dunn, *Science*, 2014, **343**, 1210–1211.
6 J. R. Miller and P. Simon, *Science*, 2008, **321**, 651.
7 G. Wang, L. Zhang and J. Zhang, *Chem. Soc. Rev.*, 2012, **41**, 797–828.
8 P. Simon and Y. Gogotsi, *Nat. Mater.*, 2008, **7**, 845–854.
9 Y. Wang, Y. Song and Y. Xia, *Chem. Soc. Rev.*, 2016, **45**, 5925–5950.
10 Y. Zhang, H. Feng, X. Wu, L. Wang, A. Zhang, T. Xia, H. Dong, X. Li and L. Zhang, *Int. J. Hydrogen Energy*, 2009, **34**, 4889–4899.
11 Z. S. Iro, *Int. J. Electrochem. Sci.*, 2016, 10628–10643.
12 G. Wang, L. Zhang and J. Zhang, *Chem. Soc. Rev.*, 2012, **41**, 797–828.
13 Y. Chai, Z. Li, J. Wang, Z. Mo and S. Yang, *J. Alloys Compd.*, 2019, **775**, 1206–1212.
14 J. Zhang, Z. Zhang, Y. Jiao, H. Yang, Y. Li, J. Zhang and P. Gao, *J. Power Sources*, 2019, **419**, 99–105.
15 C. Sengottaiyan, R. Jayavel, R. G. Shrestha, T. Subramani, S. Maji, J. H. Kim, J. P. Hill, K. Ariga and L. K. Shrestha, *Bull. Chem. Soc. Jpn.*, 2019, **92**, 521–528.
16 J. Li, Y. Wang, W. Xu, Y. Wang, B. Zhang, S. Luo, X. Zhou, C. Zhang, X. Gu and C. Hu, *Nano Energy*, 2019, **57**, 379–387.
17 J. Yang, X. Xiao, P. Chen, K. Zhu, K. Cheng, K. Ye, G. Wang, D. Cao and J. Yan, *Nano Energy*, 2019, **58**, 455–465.
18 M. F. El-Kady, Y. Shao and R. B. Kaner, *Nat. Rev. Mater.*, 2016, **1**, 16033.
19 W. Lv, Z. Li, Y. Deng, Q.-H. Yang and F. Kang, *Energy Storage Materials*, 2016, **2**, 107–138.
20 J. Jiang, Y. Li, J. Liu, X. Huang, C. Yuan and X. W. Lou, *Adv. Mater.*, 2012, **24**, 5166–5180.
21 H. Chen, J. Jiang, L. Zhang, H. Wan, T. Qi and D. Xia, *Nanoscale*, 2013, **5**, 8879–8883.
22 W. Kong, C. Lu, W. Zhang, J. Pu and Z. Wang, *J. Mater. Chem. A*, 2015, **3**, 12452–12460.
23 B. Li, M. Zheng, H. Xue and H. Pang, *Inorg. Chem. Front.*, 2016, **3**, 175–202.
24 C. Xia, P. Li, A. N. Gandi, U. Schwingenschlögl and H. N. Alshareef, *Chem. Mater.*, 2015, **27**, 6482–6485.
25 H. Wan, J. Jiang, J. Yu, K. Xu, L. Miao, L. Zhang, H. Chen and Y. Ruan, *CrystEngComm*, 2013, **15**, 7649.
26 L. Shen, L. Yu, H. B. Wu, X. Y. Yu, X. Zhang and X. W. Lou, *Nat. Commun.*, 2015, **6**, 6694.
27 X. Li and L. Zhi, *Chem. Soc. Rev.*, 2018, **47**, 3189–3216.
28 R. Raccichini, A. Varzi, S. Passerini and B. Scrosati, *Nat. Mater.*, 2015, **14**, 271–279.
29 F. Zhang, T. Zhang, X. Yang, L. Zhang, K. Leng, Y. Huang and Y. Chen, *Energy Environ. Sci.*, 2013, **6**, 1623.
30 Y. Zhai, Y. Dou, D. Zhao, P. F. Fulvio, R. T. Mayes and S. Dai, *Adv. Mater.*, 2011, **23**, 4828–4850.
31 N. Mahmood, C. Zhang, H. Yin and Y. Hou, *J. Mater. Chem. A*, 2014, **2**, 15–32.
32 X. Yu, B. Lu and Z. Xu, *Adv. Mater.*, 2014, **26**, 1044–1051.
33 P. Kulkarni, S. K. Nataraj, R. G. Balakrishna, D. H. Nagaraju and M. V. Reddy, *J. Mater. Chem. A*, 2017, **5**, 22040–22094.
34 W. Du, Z. Wang, Z. Zhu, S. Hu, X. Zhu, Y. Shi, H. Pang and X. Qian, *J. Mater. Chem. A*, 2014, **2**, 9613–9619.
35 U. Patil, S. C. Lee, S. Kulkarni, J. S. Sohn, M. S. Nam, S. Han and S. C. Jun, *Nanoscale*, 2015, **7**, 6999–7021.
36 Y. Wang, L. Wang, B. Wei, Q. Miao, Y. Yuan, Z. Yang and W. Fei, *RSC Adv.*, 2015, **5**, 100106–100113.
37 L. G. Beka, X. Li, X. Xia and W. Liu, *Diamond Relat. Mater.*, 2017, **73**, 80–86.
38 L. G. Beka, X. Li, X. Xia and W. Liu, *Diamond Relat. Mater.*, 2017, **73**, 169–176.
39 X. Wang, X. Xia, L. G. Beka, W. Liu and X. Li, *RSC Adv.*, 2016, **6**, 9446–9452.
40 M. H. Sun, S. Z. Huang, L. H. Chen, Y. Li, X. Y. Yang, Z. Y. Yuan and B. L. Su, *Chem. Soc. Rev.*, 2016, **45**, 3479–3563.
41 Z. Yu, L. Tetard, L. Zhai and J. Thomas, *Energy Environ. Sci.*, 2015, **8**, 702–730.
42 A. S. Aricò, P. Bruce, B. Scrosati, J.-M. Tarascon and W. V. Schalkwijk, *Nat. Mater.*, 2005, **4**, 366–377.

43 D. Yu, K. Goh, H. Wang, L. Wei, W. Jiang, Q. Zhang, L. Dai and Y. Chen, *Nat. Nanotechnol.*, 2014, **9**, 555–562.
44 L. Huang, D. Chen, Y. Ding, S. Feng, Z. L. Wang and M. Liu, *Nano Lett.*, 2013, **13**, 3135–3139.
45 P. Ganesan, M. Prabu, J. Sanetuntikul and S. Shanmugam, *ACS Catal.*, 2015, **5**, 3625–3637.
46 W. Dong, X. Wang, B. Li, L. Wang, B. Chen, C. Li, X. Li, T. Zhang and Z. Shi, *Dalton Trans.*, 2011, **40**, 243–248.
47 Y. Ji, X. Liu, W. Liu, Y. Wang, H. Zhang, M. Yang, X. Wang, X. Zhao and S. Feng, *RSC Adv.*, 2014, **4**, 50220–50225.
48 R. Tian, Y. Zhang, Z. Chen, H. Duan, B. Xu, Y. Guo, H. Kang, H. Li and H. Liu, *Sci. Rep.*, 2016, **6**, 19195.
49 J. Han, D. Kong, W. Lv, D.-M. Tang, D. Han, C. Zhang, D. Liu, Z. Xiao, X. Zhang, J. Xiao, X. He, F.-C. Hsia, C. Zhang, Y. Tao, D. Golberg, F. Kang, L. Zhi and Q.-H. Yang, *Nat. Commun.*, 2018, **9**, 402.
50 J. Yang, C. Yu, X. Fan, S. Liang, S. Li, H. Huang, Z. Ling, C. Hao and J. Qiu, *Energy Environ. Sci.*, 2016, **9**, 1299–1307.
51 J. Shi, X. Li, G. He, L. Zhang and M. Li, *J. Mater. Chem. A*, 2015, **3**, 20619–20626.
52 X. Gao, J. Li, D. Guan and C. Yuan, *ACS Appl. Mater. Interfaces*, 2014, **6**, 4154–4159.
53 Y. Xiao, Y. Lei, B. Zheng, L. Gu, Y. Wang and D. Xiao, *RSC Adv.*, 2015, **5**, 21604–21613.
54 Y. Zhu, Z. Wu, M. Jing, X. Yang, W. Song and X. Ji, *J. Power Sources*, 2015, **273**, 584–590.
55 F. Zhao, W. Huang, H. Zhang and D. Zhou, *Appl. Surf. Sci.*, 2017, **426**, 1206–1212.
56 L. G. Beka, X. Li and W. Liu, *J. Mater. Sci.: Mater. Electron.*, 2016, **27**, 10894–10904.
57 Y. Zhu, X. Ji, Z. Wu and Y. Liu, *Electrochim. Acta*, 2015, **186**, 562–571.
58 J. Shen, J. Wu, L. Pei, M.-T. F. Rodrigues, Z. Zhang, F. Zhang, X. Zhang, P. M. Ajayan and M. Ye, *Adv. Energy Mater.*, 2016, **6**, 1600341.
59 L.-l. Liu, K. P. Annamalai and Y.-s. Tao, *N. Carbon Mater.*, 2016, **31**, 336–342.
60 K. P. Annamalai, L. Liu and Y. Tao, *J. Mater. Chem. A*, 2017, **5**, 9991–9997.
61 S. Peng, L. Li, C. Li, H. Tan, R. Cai, H. Yu, S. Mhaisalkar, M. Srinivasan, S. Ramakrishna and Q. Yan, *Chem. Commun.*, 2013, **49**, 10178–10180.
62 Z. Gao, C. Chen, J. Chang, L. Chen, P. Wang, D. Wu, F. Xu, Y. Guo and K. Jiang, *Electrochim. Acta*, 2018, **281**, 394–404.